Supporting Information

Efficient dye-sensitized solar cells based on bioinspired copper redox mediators by tailoring counterions

Lihua Li,[a] Liang Zhao,[a] Xiao Jiang,[b] Ze Yu,*[,a] Jihong liu,[a] Hailong Rui,[a] Junyu Shen,*[,c] Walid Sharmoukh,[d] Nageh K. Allam,[e] and Licheng Sun[a,f,g]

[a]State Key Laboratory of Fine Chemicals, Dalian University of Technology (DUT), Dalian 116024, China.

[b]Key Laboratory of Industrial Ecology and Environmental Engineering (Ministry of Education), School of Environmental Science and Technology, Dalian University of Technology, Dalian 116024, China.

[c]Jiangsu Laboratory of Advanced Functional Materials, School of Materials Engineering, Changshu Institute of Technology, Changshu 215500, China.

[d]Department of Inorganic Chemistry, National Research Centre, Dokki, Giza 12622, Egypt.

[e]Energy Materials Laboratory (EML), School of Sciences and Engineering, The American University in Cairo, New Cairo 11835, Egypt.

[f]Department of Chemistry, School of Engineering Sciences in Chemistry, Biotechnology and Health, KTH Royal Institute of Technology, Stockholm 10044, Sweden.

[g]Center of Artificial Photosynthesis for Solar Fuels, School of Science, Westlake University, 310024 Hangzhou, China.

Additional Experimental Details

Materials. $CuSO_4 \cdot 5H_2O$, $Cu(PF_6) \cdot 4CH_3CN$, $Cu(BF_4)_2 \cdot 6H_2O$, $Cu(BF_4) \cdot 4CH_3CN$, $n NH_4PF_6$, K_2CO_3, acetonitrile, diethyl ether, ethanedithiol, 2-(chloromethyl)pyridine, 4-*tert*-butylpyridine, 2,6-di-tert-butylpyridine, and lithium bis(trifluoromethanesulfonyl)imide were purchased from Adamas reagent and used as received. The platinum wire and glassy carbon electrode were purchased from Tianjin Gaoss Union for the electrochemical studies. $[Cu^{(II/I)}(tmby)_2]$ $TFSI_{2/1}$ (tmby = bis-(4,4',6,6'-tetramethyl-2,2'-bipyridine)) redox shuttles and dye 3-{6-{4-[bis(2',4'-dihexyloxybiphenyl-4-yl)amino-]phenyl}-4,4-dihexyl-cyclopenta-[2,1-b:3,4-b']dithiphene-2-yl}-2-cyanoacrylic acid (Y123) were purchased from Dyenamo AB in Sweden.

Instruments. Powder X-ray diffraction (PXRD) measurements were obtained on a Riguku D/Max-2,400 XRD instrument with a sealed Cu tube (λ = 1.54178 Å). Mass spectra were recorded with HP 1100 HPL/ESI-DAD-MS and Waters/Micromass LC/Q-TOF-MS instruments. Elemental analyses were performed with a Thermoquest-Flash EA 1112 elemental analyzer. UV-vis absorption measurements were carried out on an Agilent 8453 spectrophotometer. The test optical path length was 1 cm. NMR spectra were collected with a Varian INOVA 400 NMR spectrometer. Cyclic voltammetry was measured by a model CHI660E electrochemical workstation (CH instruments). The Photocurrent Density-Voltage Plots of the devices were obtained by a Keithley 2400 Source-Meter under a simulate irradiation (100 mW/cm^2, AM 1.5G) provided by Sol3A Class AAA Solar Simulator with a 450 Watt Xenon source and irradiation area 2 × 2 in. illuminated area. A Newport provided standard Silica-based reference cell were

used to calibrate the irradiation strength. The solar cell scan rate is 50 mV/s. The fabrication and testing of DSCs are carried out under room temperature conditions. Electrochemical impedance spectroscopy (EIS) was measured using a Zennium analyzer system (Model: IM6, Zahner, German) in a frequency range from 10^6 Hz to 0.1 Hz. Nanosecond transient absorption spectra (TAS) were recorded with an Edinburgh LP920 transient absorption spectrometer. The excitation wavelength was 532 nm and probe wavelength was 720 nm. The incident photon-to-current conversion efficiency (IPCE) spectra were obtained from the Hypermonolight (SM–25, Japan), using a standard silicon solar cell to calibrate before test. The integral current is calculated as follows: $JIPCE = \int_{\lambda 2}^{\lambda 1} IPCE(\lambda) \cdot e \cdot \Phi in(\lambda) d\lambda$, Φ_{in} and e are incident photon flux and electron elementary charge, respectively.

Crystallographic Structure Determinations. The single-crystal X-ray diffraction data were collected on a Bruker Smart Apex II CCD diffractometer with a graphite-monochromated Mo-K_α radiation (λ = 0.071073 Å) at 296 K using the ω-2θ scan mode. Data processing was accomplished with the SAINT processing program.[1] Intensity data were corrected for absorption by the SADABS program.[2] All structures were solved by direct methods and refined on F^2 against full-matrix least-squares methods by using the SHELXTL 97 program package.[3] Non-hydrogen atoms were refined anisotropically. Hydrogen atoms were located by geometrical calculation. Crystallographic data and selected bond lengths and angles for $[Cu(N_2S_2)(CH_3CN)](BF_4)_2$, $[Cu(N_2S_2)(CH_3CN)](PF_6)_2$, $[Cu(N_2S_2)]_n(BF_4)_n$, and $[Cu(N_2S_2)]_2(PF_6)_2$ are given in

Tables S1 and Table S2 (CCDC–2020090, CCDC–2097665, CCDC–2097667, and CCDC–2097669).

Device Fabrication. The DSC devices were fabricated as reported previously.[4-6] First, fluorine-doped tin oxide (FTO) conducting glasses (Pilkington, TEC 15) were sequentially cleaned by detergent, deionized water, and ethanol for 30 min, respectively. The cleaned FTO glasses were soaked in 40 mM $TiCl_4$ aqueous solution at 70 ℃ for 30 min, and then sintered at 500 ℃ for 30 min. DSC devices were constructed with a double layer TiO_2 film consisting of a ~6 μm transparent layer and a ~4 μm scatting layer. The transparent layer was fabricated by screen-printing of TiO_2 18NR-T paste three times, every time dried at 130 ℃ for 5 min, and the scattering layer was fabricated by screen-printing of TiO_2 TPP200 paste one time. After sintering at 500 ℃ for 30 min, the TiO_2 films were treated with $TiCl_4$ aqueous solution at 70 ℃ for 30 min again. The sintered photoanode TiO_2 films were immersed into a 0.1 mM Y123 dye solution in acetonitrile and *tert*-butanol mixed solvent (1:1, v/v) overnight containing 0.5 mM chenodeoxycholic acid. The unattached dyes were rinsed by ethanol and acetonitrile. The Pt counter electrodes are purchased from Heptachroma and used as received. The counter electrode poly(3,4-ethylenedioxythiophene) (PEDOT) was prepared by an electrodeposition method as reported previously.[7] The dye-sensitized TiO_2 photoanode and counter electrode Pt were assembled by a 25 μm Surly film. The liquid electrolyte was injected into the interlayer by a predrilled hole, which was then sealed with a Surlyn film and a glass cover. The active area of the DSC devices was 0.16 cm^2. The photocurrent density-voltage measurements were performed with a black mask (1 mm wider than the active area).

Determination of the concentrations of saturated solutions for Cu(I) complexes.

(a) Draw the standard curves of $[Cu(N_2S_2)]_n(BF_4)_n$ and $[Cu(N_2S_2)]_2(PF_6)_2$ at the concentrations from 0.01 to 0.30 mM: $A_{PF6} = 7.54 \times c_{PF6} - 0.01$; $A_{BF4} = 8.33 \times c_{BF4} - 0.01$. ($A$ is the absorbing intensity; c is the the concentration)

(b) Prepare the saturated solutions of $[Cu(N_2S_2)]_n(BF_4)_n$, and $[Cu(N_2S_2)]_2(PF_6)_2$ in acetonitrile and filter insoluble solid.

(c) Dilute the saturated solution 1000 times and collect their absorbance in UV-vis spectra.

(d) Calculate the concentrations of saturated solutions for Cu(I) complexes based on the standard curves.

Electrochemistry Studies. All electrochemical measurements were performed with a model CHI660E electrochemical workstation (CH instruments). Cyclic voltammetry experiments were carried out in a three-electrode cell under argon. The working electrode was a glassy carbon (GC) electrode (0.071 cm^2), the reference electrode was a non-aqueous Ag^+/Ag (0.01 M $AgNO_3$ in CH_3CN) electrode, and the counter electrode was a platinum wire. A solution of 0.1 M nBu$_4$NPF$_6$ in CH_3CN was used as a supporting electrolyte, which was degassed by bubbling with argon for 15 min before measurement. The ferricinium/ferrocene ($Fc^{+/0}$) couple was used as an internal reference and the Ag^+/Ag electrode is corrected by the $Fc^{+/0}$ potential ($E_{(Fc+/0)}$ = 0.64 V vs NHE).

(a)

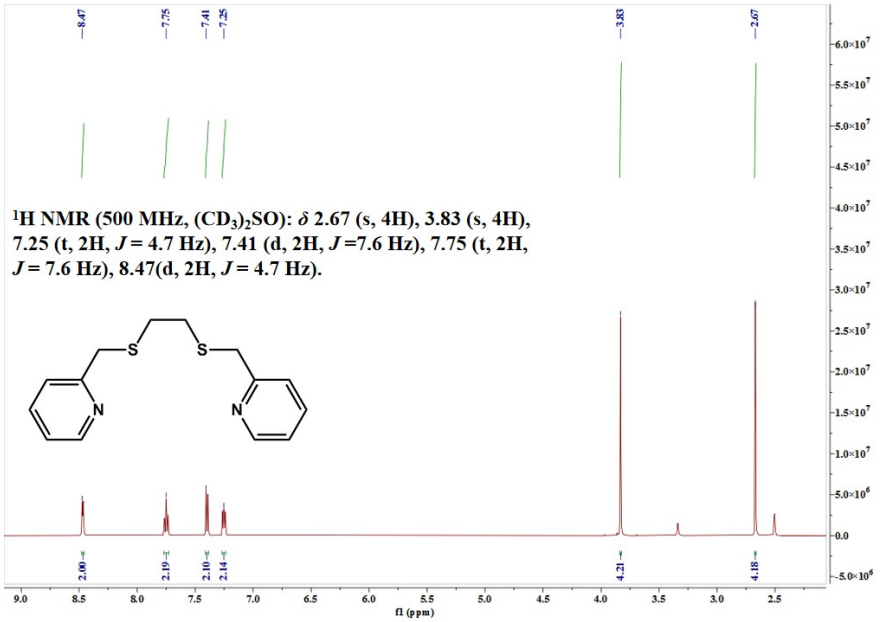

^{1}H NMR (500 MHz, $(CD_3)_2SO$): δ 2.67 (s, 4H), 3.83 (s, 4H), 7.25 (t, 2H, J = 4.7 Hz), 7.41 (d, 2H, J =7.6 Hz), 7.75 (t, 2H, J = 7.6 Hz), 8.47(d, 2H, J = 4.7 Hz).

(b)

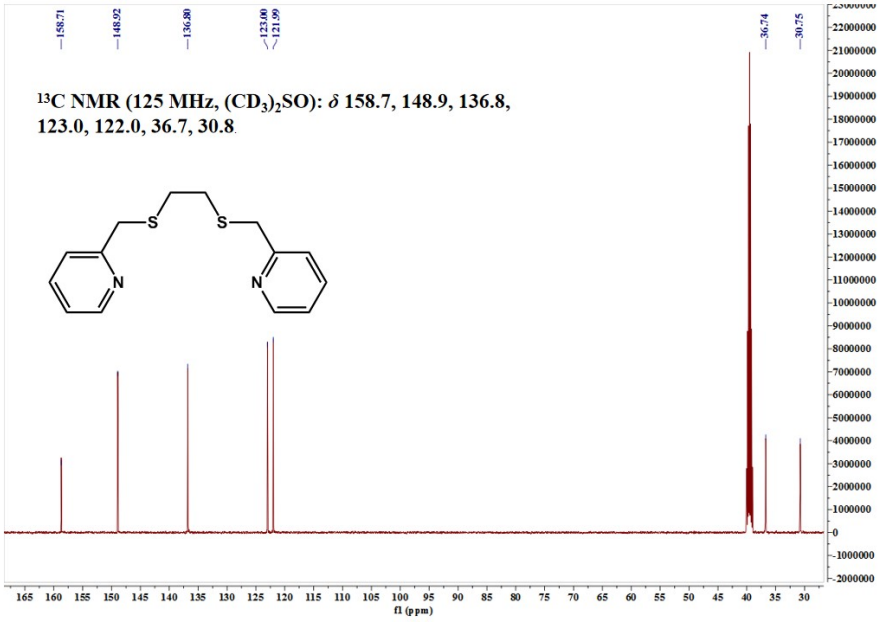

^{13}C NMR (125 MHz, $(CD_3)_2SO$): δ 158.7, 148.9, 136.8, 123.0, 122.0, 36.7, 30.8.

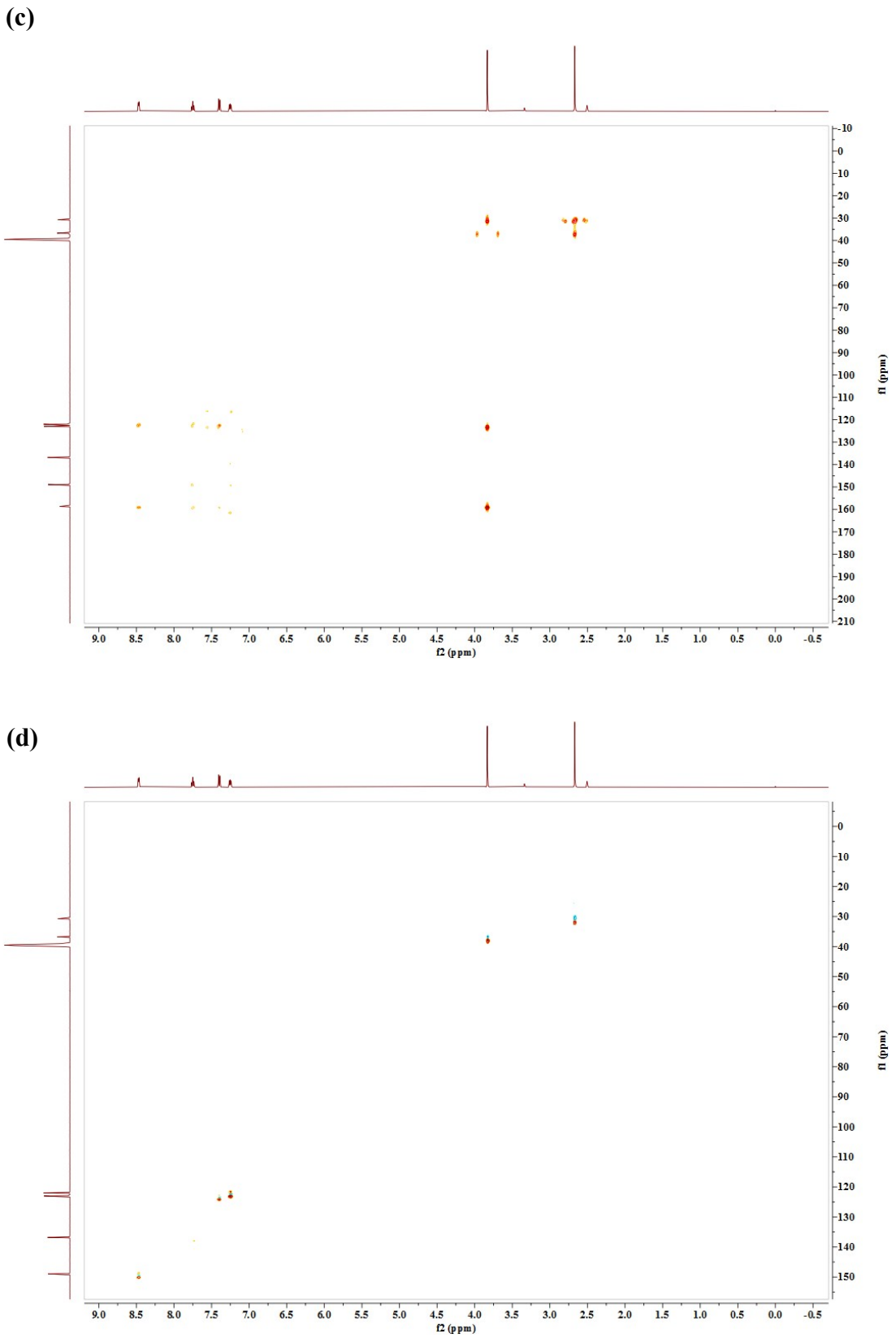

Fig. S1. (a) ^{1}H NMR, (b)^{13}C NMR, (c) HMBC NMR, and (d) HSQC NMR spectra of N_2S_2 in $(CD_3)_2SO$.

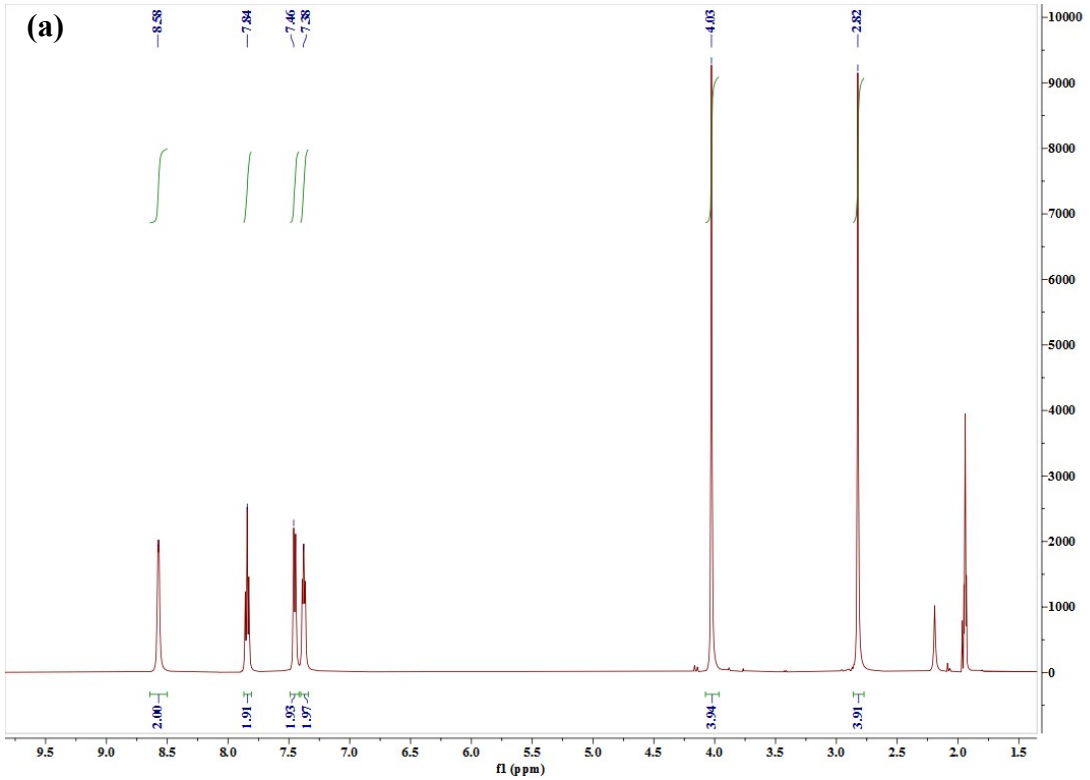
(a)
8.58
7.84
7.46
7.38
4.03
2.82
2.00
1.91
1.93
1.97
3.94
3.91
f1 (ppm)

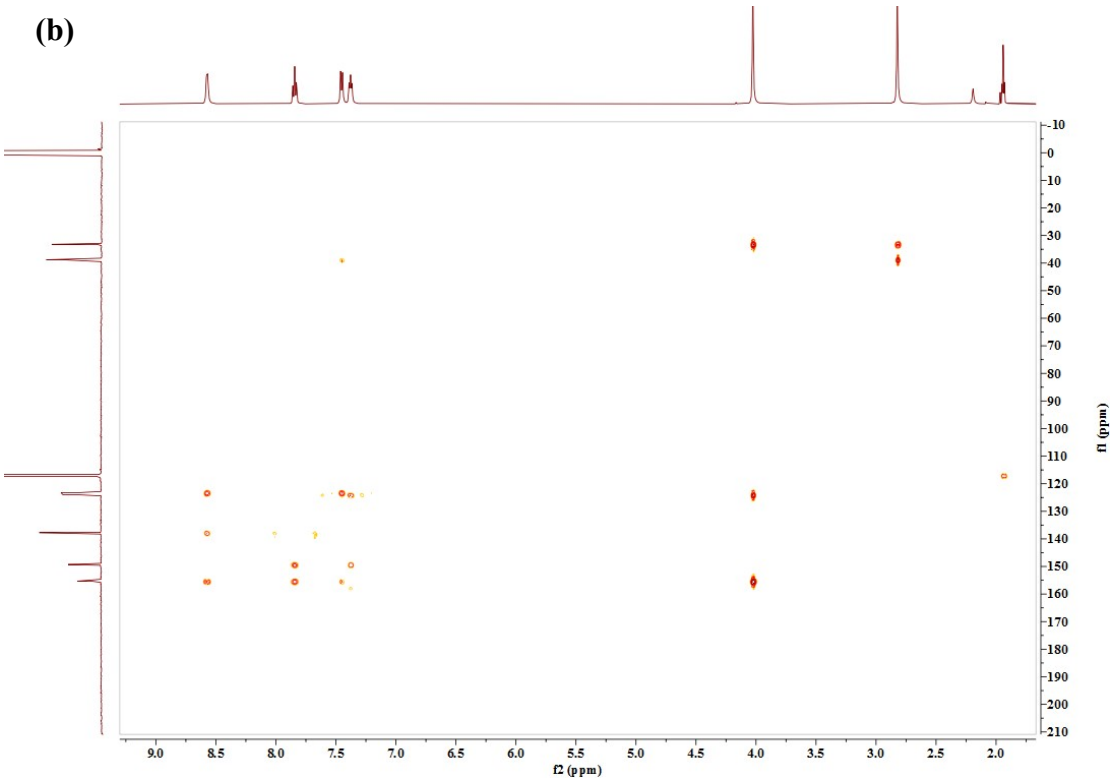
(b)
f2 (ppm)
f1 (ppm)

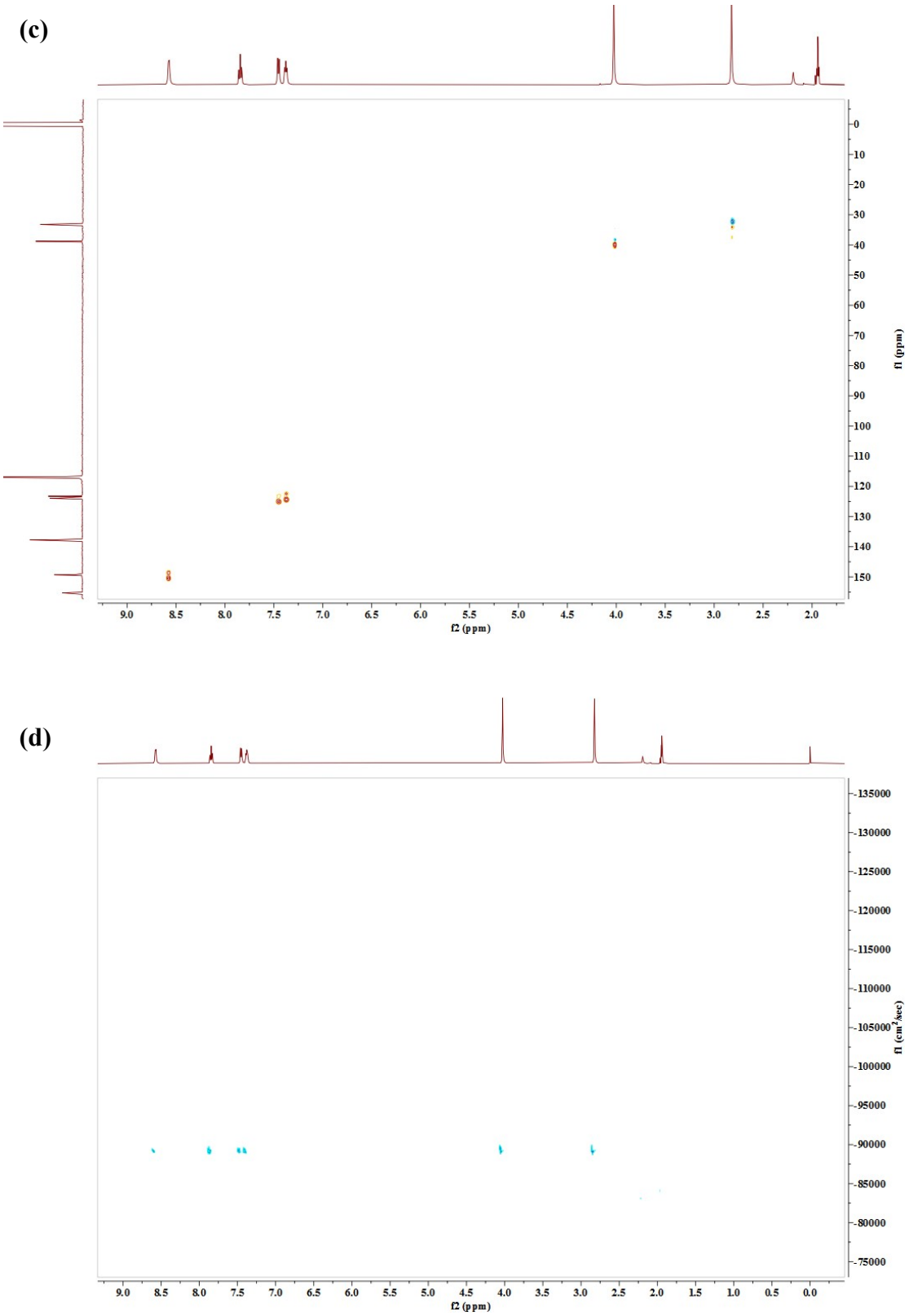

Fig. S2. (a) ^{1}H NMR, (b) HMBC NMR, (c) HSQC NMR and (d) DOSY NMR spectra of $[Cu(N_2S_2)]_n(BF_4)_n$ in CD_3CN.

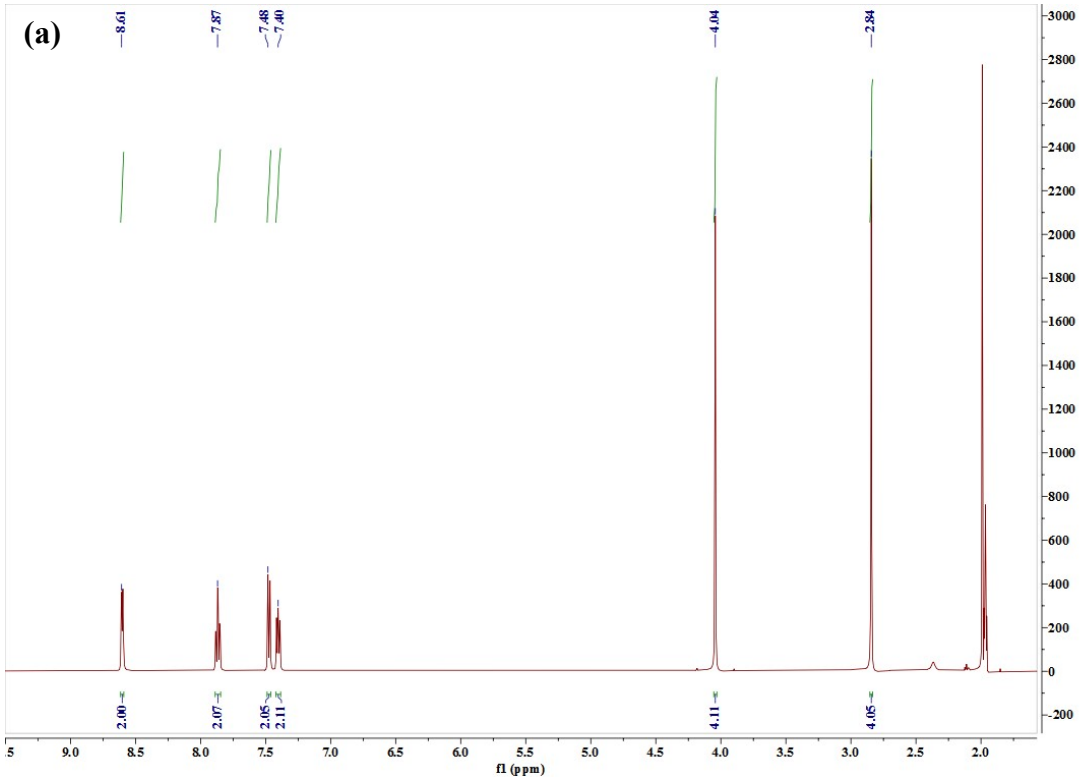
(a)
8.61
7.87
7.48
7.40
4.04
2.84
2.00
2.07
2.05
2.11
4.11
4.05
f1 (ppm)

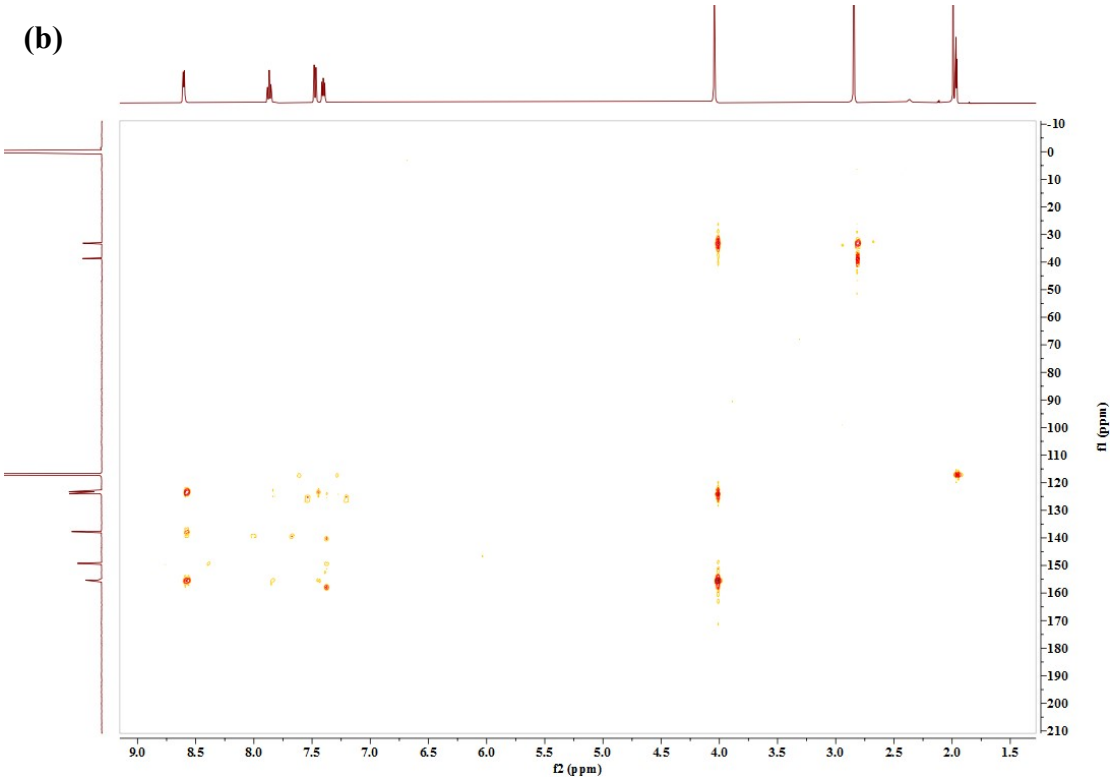
(b)
f2 (ppm)
f1 (ppm)

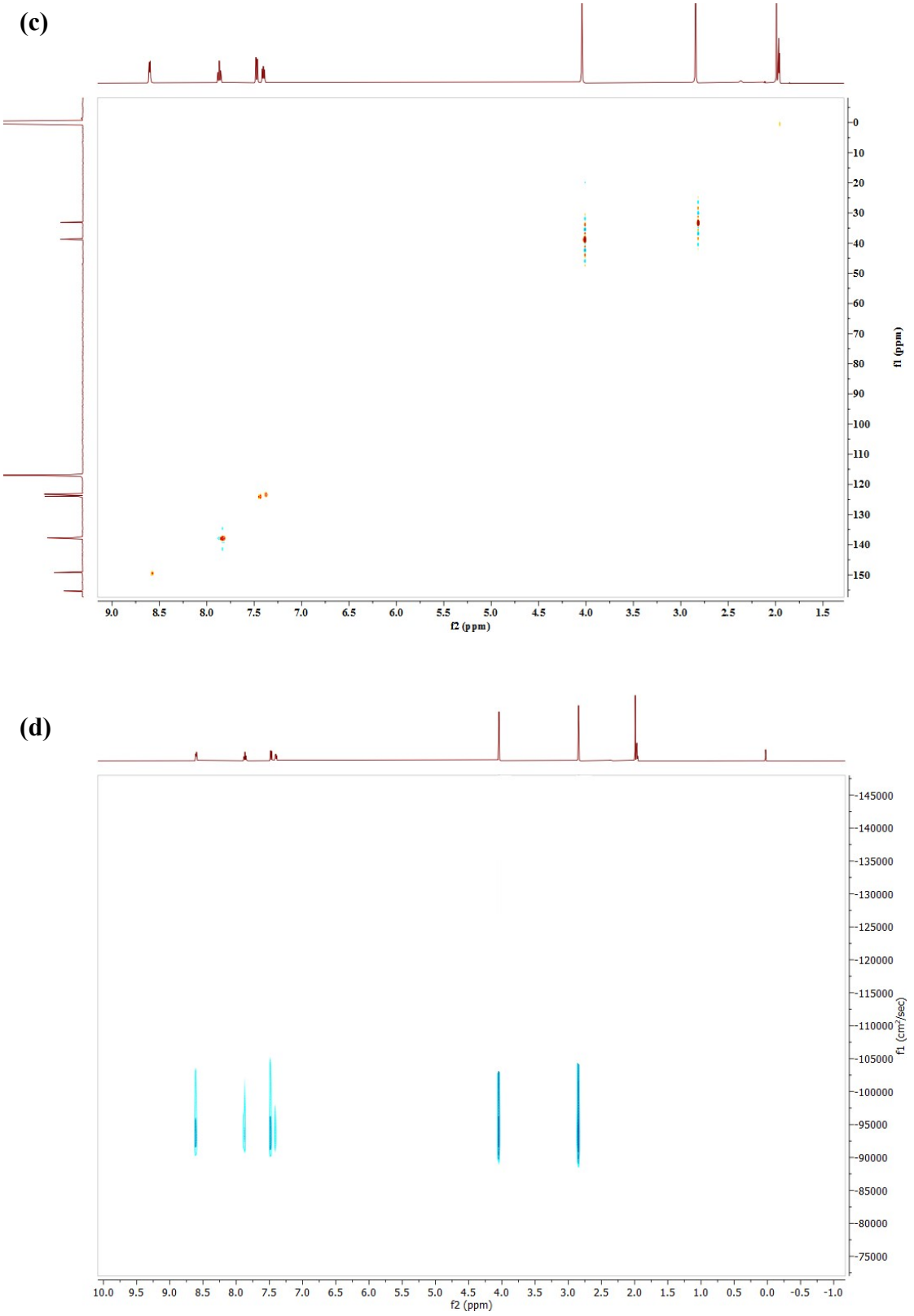

Fig. S3. (a) ^{1}H NMR, (b) HMBC NMR, (c) HSQC NMR, and (d) DOSY NMR spectra of $[Cu(N_2S_2)]_2(PF_6)_2$ in CD_3CN.

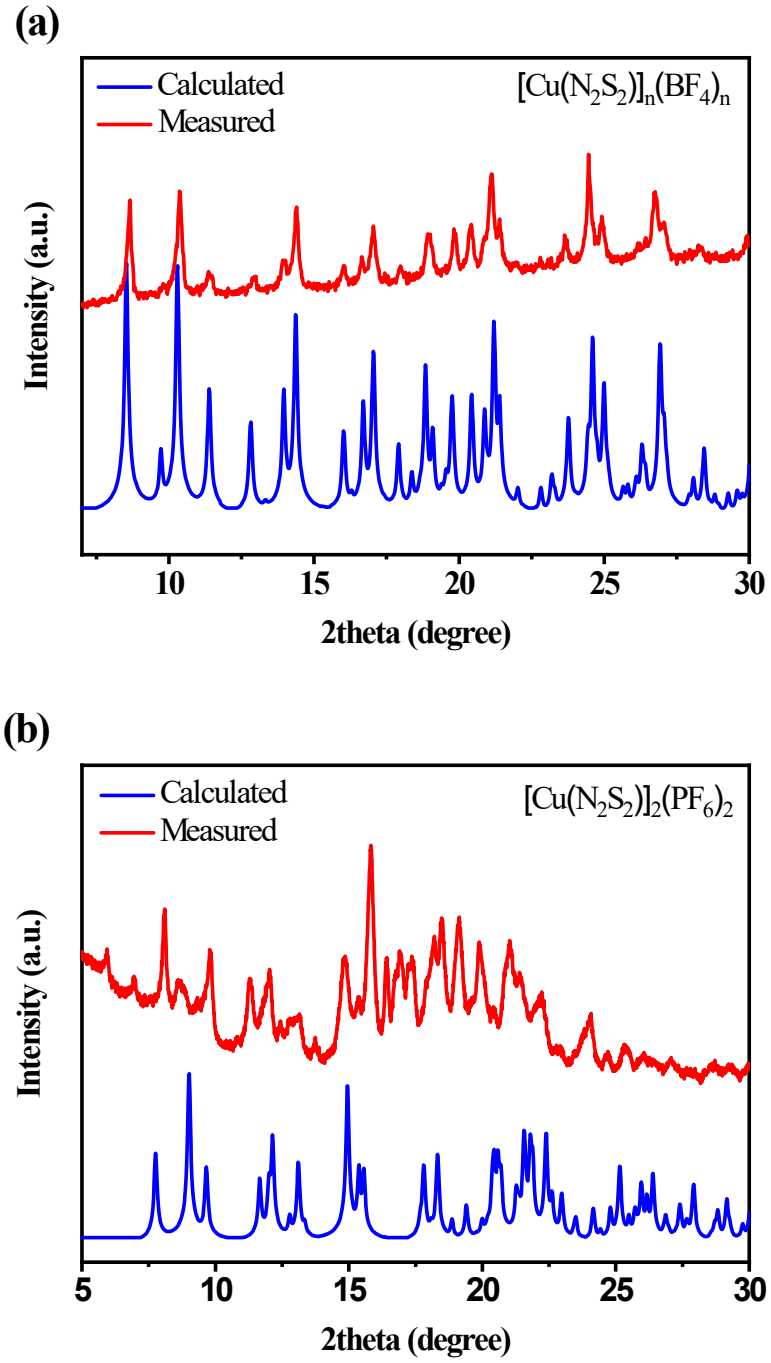

Fig. S4. PXRD and calculated patterns based on the single-crystal simulation for (a) $[Cu(N_2S_2)]_n(BF_4)_n$ and (b) $[Cu(N_2S_2)]_2(PF_6)_2$.

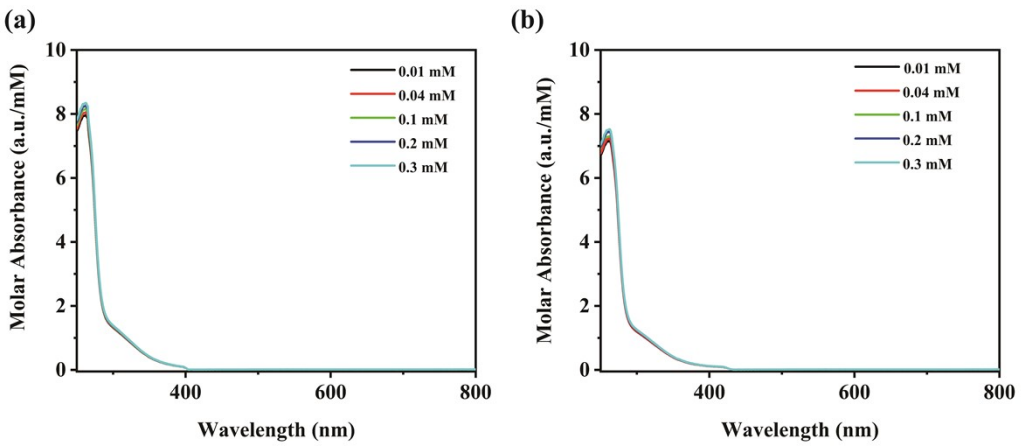

Fig. S5. UV-vis absorption spectra of (a) $[Cu(N_2S_2)]_n(BF_4)_n$ and (b) $[Cu(N_2S_2)]_2(PF_6)_2$ at different concentrations (optical length is 1 mm).

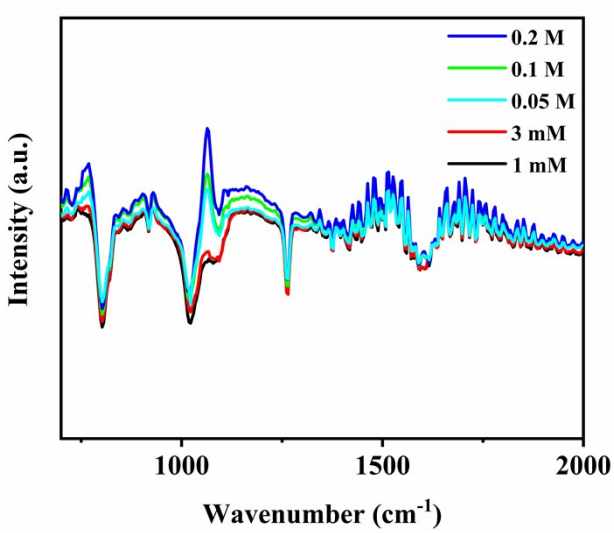

Fig. S6. In-situ FT-IR spectra of $[Cu(N_2S_2)]_n(BF_4)_n$ during the dilution process with varied concentrations.

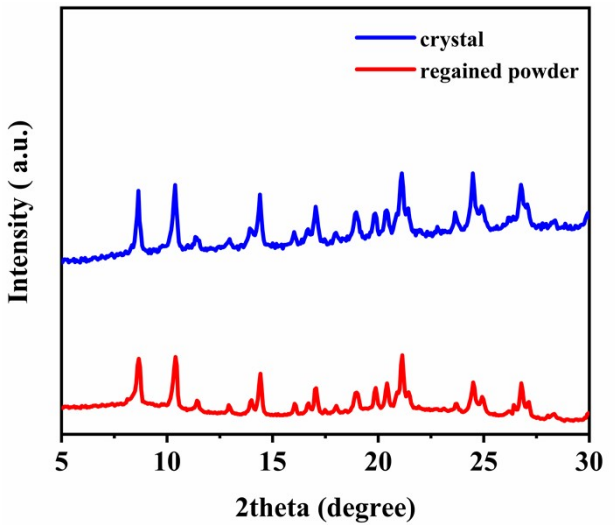

Fig. S7. PXRD of pure $[Cu(N_2S_2)]_n(BF_4)_n$ crystal and regained $[Cu(N_2S_2)]_n(BF_4)_n$ powder after staying in acetonitrile for 3 days.

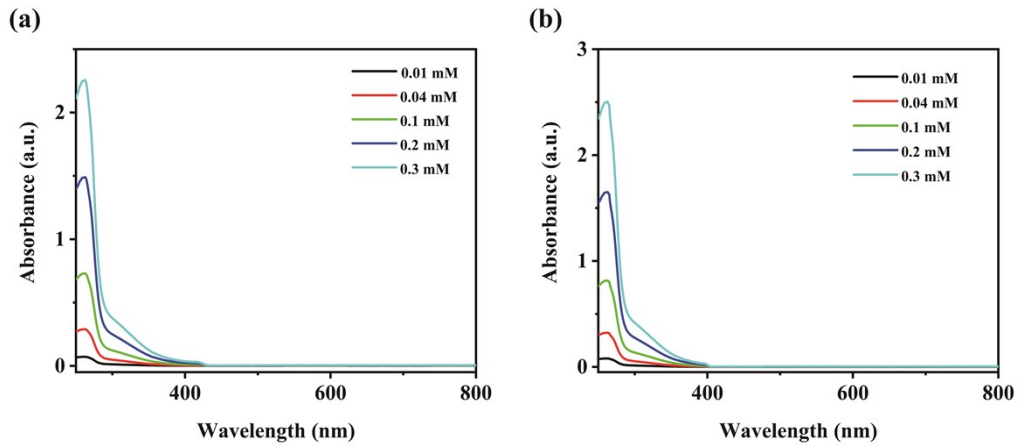

Fig. S8. UV-vis spectra of (a) $[Cu(N_2S_2)]_2(PF_6)_2$ and (b) $[Cu(N_2S_2)]_n(BF_4)_n$ in acetonitrile solutions with the concentrations varied from 0.01 to 0.30 mM (optical length is 1 mm).

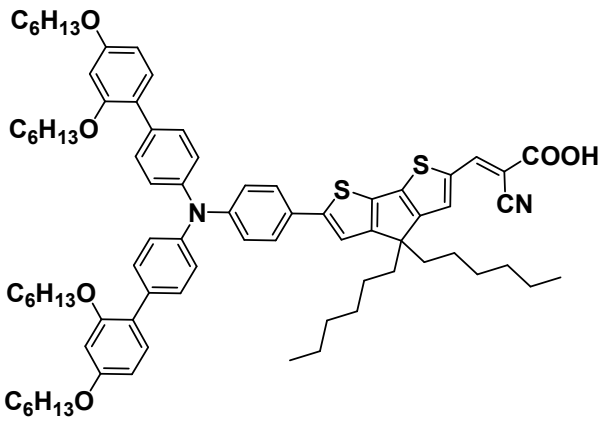

Fig. S9 Molecular structure of dye Y123.

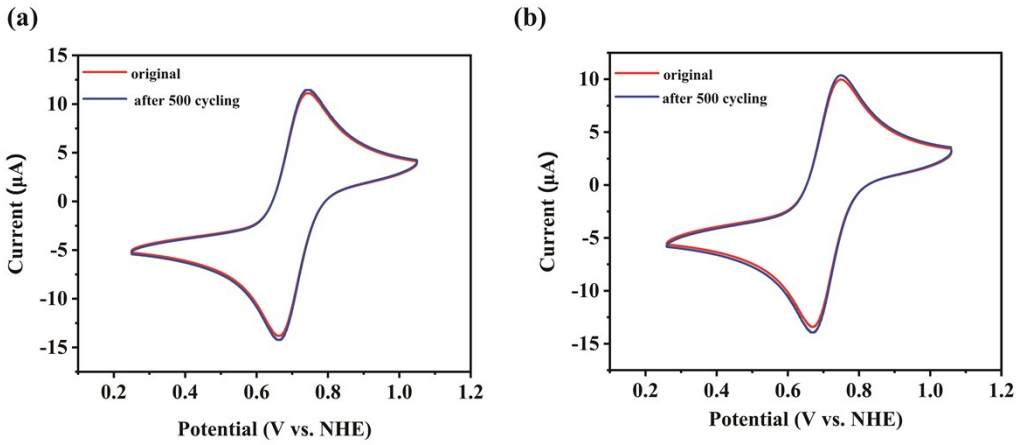

Fig. S10. Cyclic voltammograms of (a) $[Cu(N_2S_2)]_n(BF_4)_n$ and (b) $[Cu(N_2S_2)(CH_3CN)](BF_4)_2$ (both at 1 mM) in acetonitrile solution containing 0.1 M nBu$_4$NPF$_6$ at a scan rate of 50 mV s^{-1} after 500 times scanning.

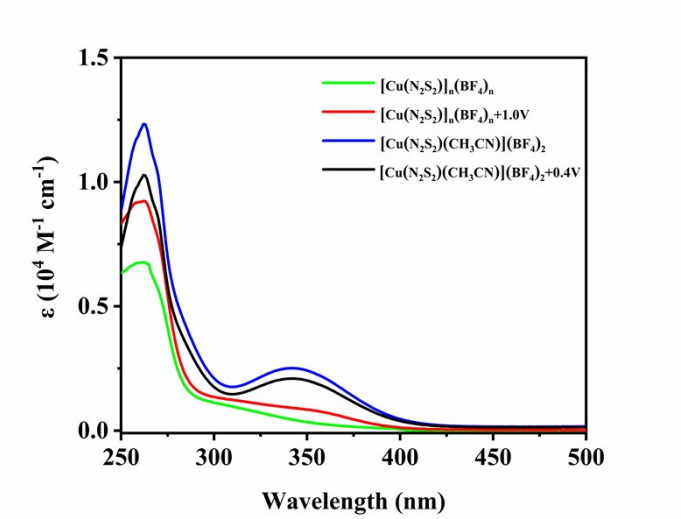

Fig. S11. The spectroelectrochemistry of $[Cu(N_2S_2)]_n(BF_4)_n$ at 1.0 V vs. NHE and $[Cu(N_2S_2)(CH_3CN)](BF_4)_2$ at 0.4 V vs. NHE in acetonitrile solutions containing 0.1 M nBu$_4$NPF$_6$ (optical length is 1 mm).

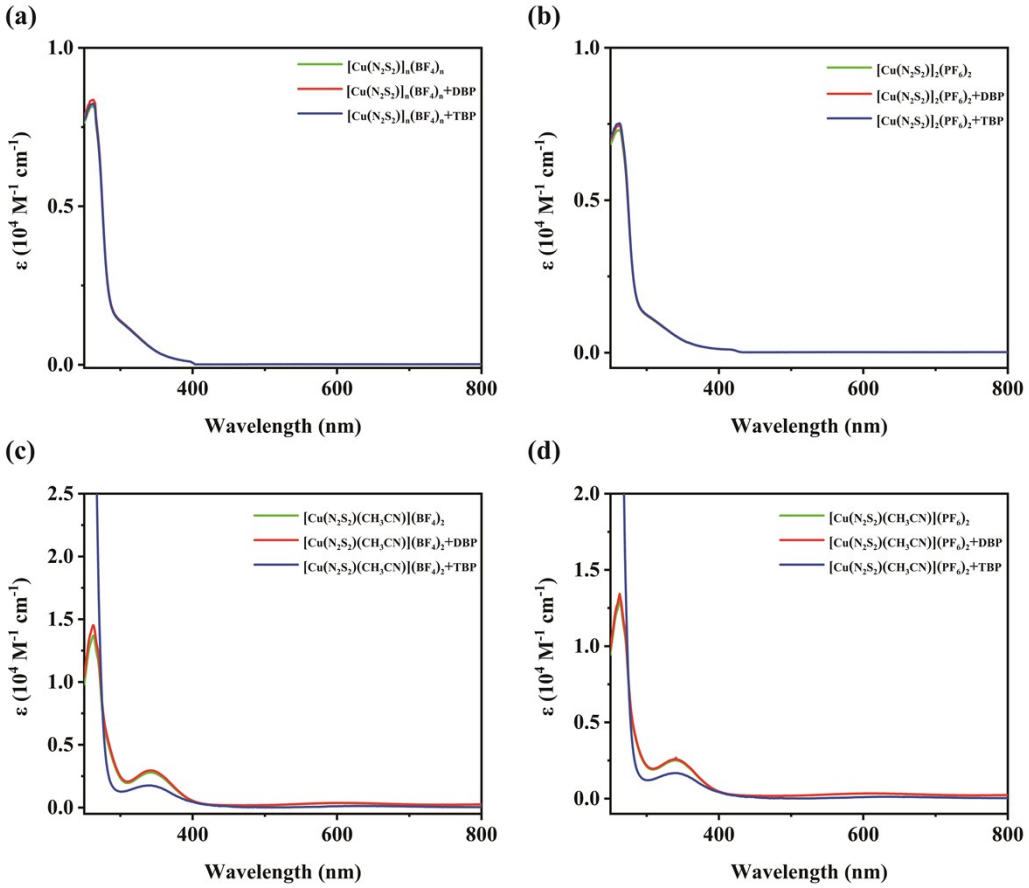

Fig. S12. UV-vis spectra of (a) $[Cu(N_2S_2)]_n(BF_4)_n$, (b) $[Cu(N_2S_2)]_2(PF_6)_2$, (c) $[Cu(N_2S_2)(CH_3CN)](BF_4)_2$, and (d) $[Cu(N_2S_2)(CH_3CN)](PF_6)_2$ (all in 0.1 mM) with 10 molar eq. of DBP or TBP in acetonitrile.

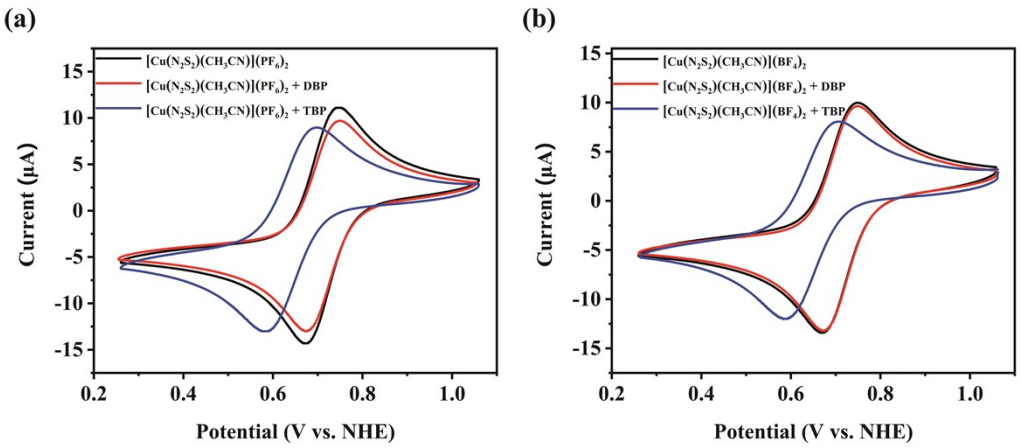

Fig. S13. Cyclic voltammograms of (a) $[Cu(N_2S_2)(CH_3CN)](PF_6)_2$ and (b) $[Cu(N_2S_2)(CH_3CN)](BF_4)_2$ (both at 1 mM) with 5 molar eq. of TBP or DBP in acetonitrile solution containing 0.1 M nBu$_4$NPF$_6$ at a scan rate of 50 mV s^{-1}.

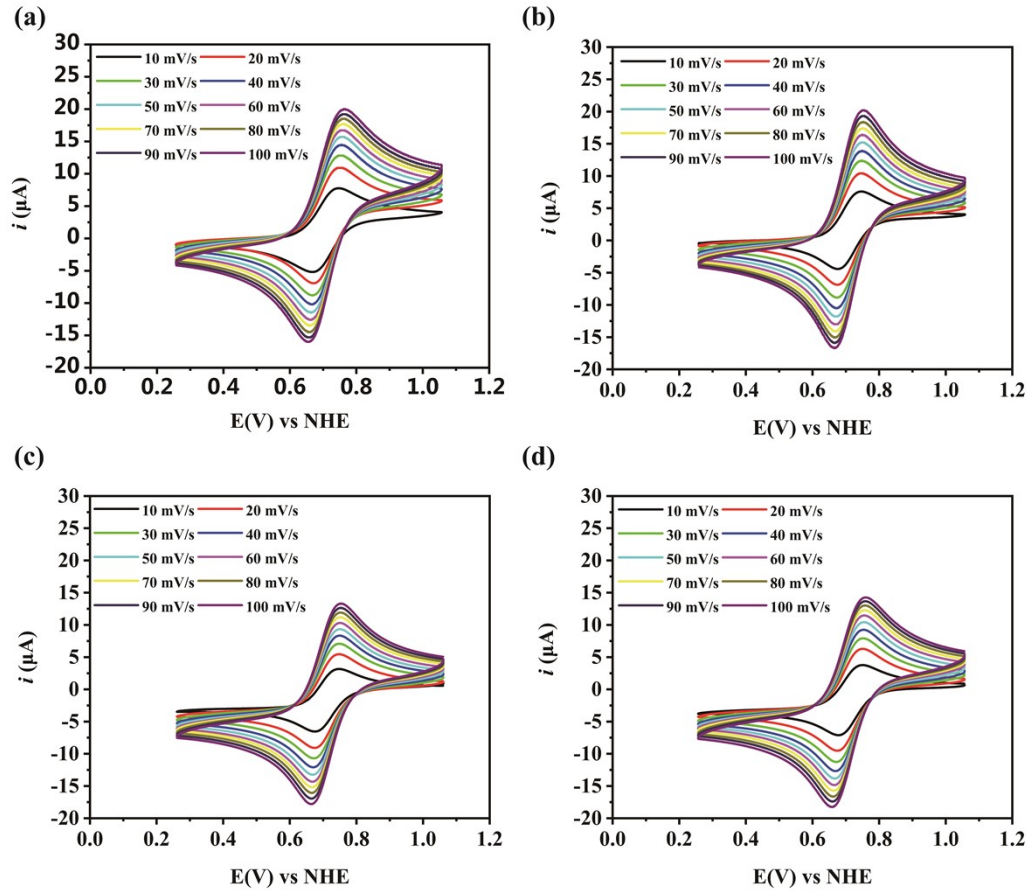

Fig. S14. Cyclic voltammograms of (a) $[Cu(N_2S_2)]_n(BF_4)_n$, (b) $[Cu(N_2S_2)]_2(PF_6)_2$, (c) $[Cu(N_2S_2)(CH_3CN)](BF_4)_2$ and (d) $[Cu(N_2S_2)(CH_3CN)](PF_6)_2$ (all in 1 mM) in 0.1 M nBu$_4$NPF$_6$ in acetonitrile at different scan rates from 10 mV/s to 100 mV/s.

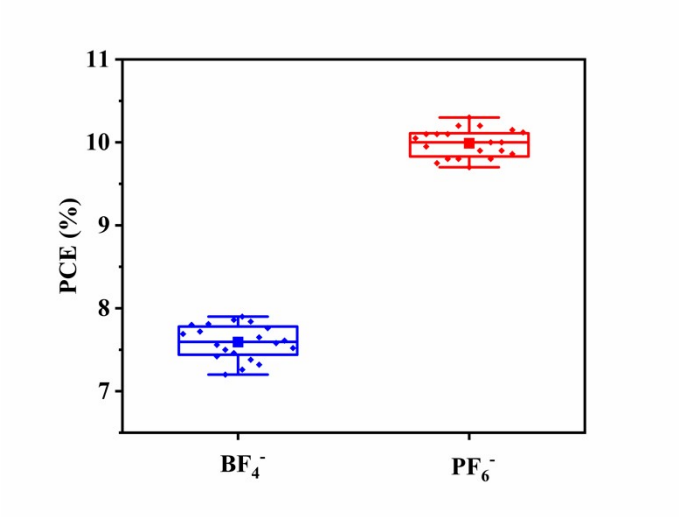

Fig. S15. Photovoltaic parameters of the DSC devices based on electrolytes E1 and E2. Error bars represent minimum and maximum values, and the middle line in each box represents the median value, filled squares indicate mean values. Each box data from 20 devices for each eleltrolytes is presented.

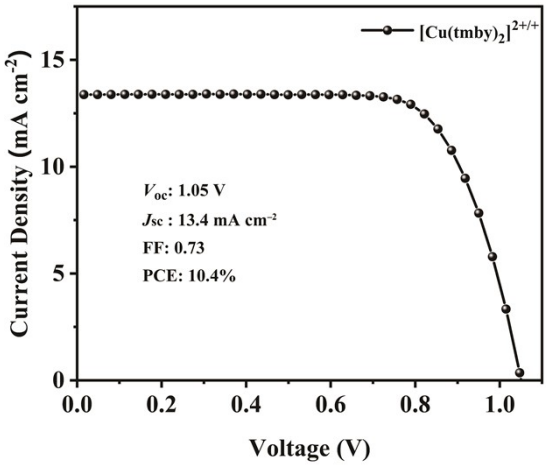

Fig. S16. *J*–*V* curves of the best DSCs containing $[Cu(tmby)_2]^{2+/+}$ electrolytes (0.25 M Cu(I), 0.06 M Cu(II), 0.1 M LiTFSI and 0.6 M TBP) in acetonitrile measured under illumination (100 mW cm^{-2} , AM 1.5G).

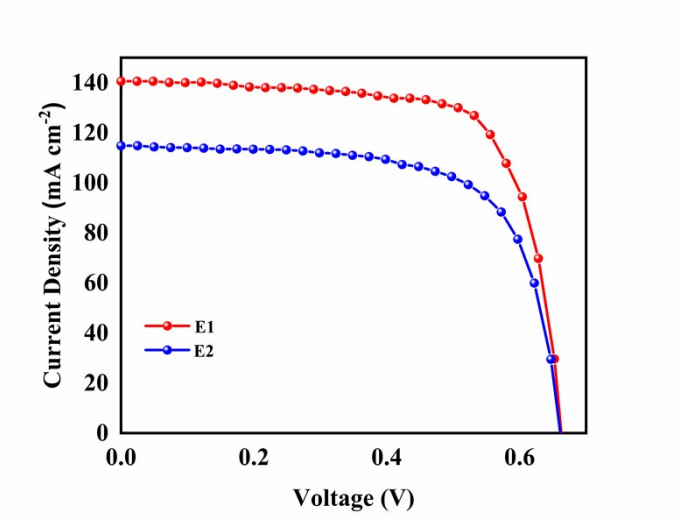

Fig. S17. Photovoltaic characteristics of DSCs measured under indoor-light conditions at 1000 lux with E1 (0.15 M Cu(I), 0.0375 M Cu(II)) and E2 (0.07 M Cu(I), 0.0175M Cu(II)) with 0.5 M DBP, 0.1 M Li-TFSI, and 0.01 M CDCA in acetonitrile. The DSCs fabricated for the study of indoor-light conditions have a larger area of 1 cm^2.

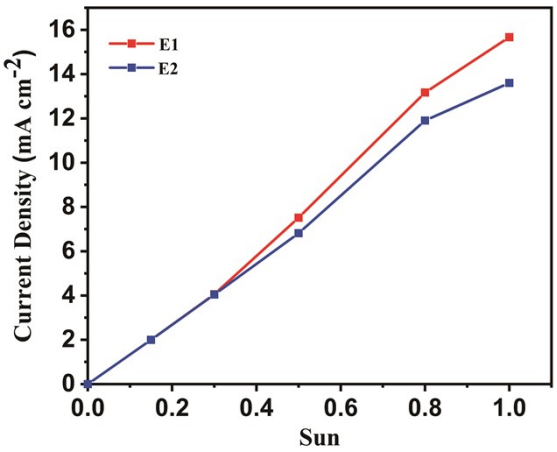

Fig. S18. Light intensity dependence of short-circuit current density for DSCs based on the two different copper electrolytes.

Table S1. Crystallographic data and processing parameters for $[Cu(N_2S_2)(CH_3CN)](BF_4)_2$, $[Cu(N_2S_2)(CH_3CN)](PF_6)_2$, $[Cu(N_2S_2)]_n(BF_4)_n$, and $[Cu(N_2S_2)]_2(PF_6)_2$.

Complex	$[Cu(N_2S_2)(CH_3CN)](BF_4)_2$	$[Cu(N_2S_2)(CH_3CN)](PF_6)_2$	$[Cu(N_2S_2)]_n(BF_4)_n$	$[Cu(N_2S_2)]_2(PF_6)_2$
Formula	$C_{16}H_{19}N_3S_2B_2F_8Cu$	$C_{38}H_{47}N_8S_4P_4F_{24}Cu_2$	$C_{14}H_{16}N_2S_2BF_4Cu$	$C_{16}H_{19}N_3S_2PF_6Cu$
Formula weight	554.62	1465.06	426.76	525.97
Crystal system	Monoclinic	Triclinic	Monoclinic	Triclinic
Space group	*P2(1)/c*	*P-1*	*P2(1)/c*	*P-1*
Z	4	2	4	2
a / Å	12.7700(3)	13.4399(8)	10.0136(2)	9.1674(4)
b / Å	17.4754(3)	13.5650(8)	15.1324(4)	9.8123(4)
c / Å	10.4435(2)	15.9193(9)	10.8645(2)	11.4150(5)
α / deg	90.00	89.652(2)	90.00	92.2690(10)
β / deg	107.450(2)	87.434(2)	92.6970(10)	93.6030(10)
γ / deg	90.00	74.450(2)	90.00	90.8780(10)
V / Å^3	2223.32(8)	2793.2(3)	1644.47(6)	1023.82(8)
D_{calcd} / g m^{-3}	1.657	1.74	1.724	1.706
μ / mm^{-1}	1.246	1.142	1.622	1.410
Crystal size / mm	0.23 × 0.20 × 0.17	0.25 × 0.21 × 0.19	0.21 × 0.20 × 0.19	0.25 × 0.17 × 0.09
θ Range / deg	2.04 / 27.48	2.253 / 32.796	2.31 / 31.67	2.94 / 30.50
Reflns collected/Indep.	5064 / 2790	16352 / 12325	2883 / 2489	3138 / 2984
Parameters refined	290	720	225	263
F(000)	1116	1349	864	532
GOF on F^2	1.078	1.042	1.035	1.046
Final R_1 ($I > 2(I)$)	0.0602	0.0593	0.0272	0.0321
Final wR_2 ($I > 2(I)$)	0.1672	0.1585	0.0664	0.0812
max. peak/hole / e Å^{-3}	1.006 / -0.797	1.729 / -1.036	0.456 / -0.376	0.795 / -0.578

$R_1 = \Sigma||F_o| - |F_c||/\Sigma|F_o|$, $wR_2 = [\Sigma(|F_o|^2 - |F_c|^2)^2/\Sigma(Fo_2)]^{1/2}$

Table S2 Selected bond lengths (Å) and angles (deg) for $[Cu(N_2S_2)(CH_3CN)](BF_4)_2$, $[Cu(N_2S_2)(CH_3CN)](PF_6)_2$, $[Cu(N_2S_2)]_n(BF_4)_n$, and $[Cu(N_2S_2)]_2(PF_6)_2$.

$[Cu(N_2S_2)(CH_3CN)](BF_4)_2$		$[Cu(N_2S_2)(CH_3CN)](PF_6)_2$		$[Cu(N_2S_2)]_n(BF_4)_n$		$[Cu(N_2S_2)]_2(PF_6)_2$	
Bond Length (Å)		Bond Length (Å)		Bond Length (Å)		Bond Length (Å)	
Cu–N1	1.990(5)	Cu–N1	1.992(2)	Cu–N1	2.057(3)	Cu–N1	2.081(8)
Cu–N2	1.987(3)	Cu–N2	1.995(3)	Cu–N2	1.992(4)	Cu–N2	1.990(1)
Cu–N3	2.015(9)	Cu–N3	1.995(3)	Cu–S1	2.349(8)	Cu–S1	2.364 (1)
Cu–S1	2.409(6)	Cu–S1	2.462(0)	Cu–S2	2.374(2)	Cu–S2	2.298(2)
Cu–S2	2.390(9)	Cu–S2	2.335(4)				
Bond Angle (deg)		Bond Angle (deg)		Bond Angle (deg)		Bond Angle (deg)	
N1–Cu–N2	174.52(3)	N1–Cu–N2	174.33(6)	N1–Cu–N2	117.86(7)	N1–Cu1–N2	112.90(9)
N1–Cu–N3	91.44(3)	N1–Cu–N3	90.56(2)	N1–Cu–S1	87.35(5)	N1–Cu1–S1	86.02(0)
N1–Cu–S1	84.75(4)	N1–Cu–S1	85.17(7)	N1–Cu–S2	100.98(5)	N1–Cu1–S2	108.41(8)
N1–Cu–S2	90.18(2)	N1–Cu–S2	88.37(5)	N2–Cu–S1	132.11(5)	N2–Cu1–S1	118.83(7)
N2–Cu–N3	93.82(4)	N2–Cu–N3	95.09(9)	N2–Cu–S2	121.91(6)	N2–Cu1–S2	128.82(6)
N2–Cu–S1	92.75(0)	N2–Cu–S1	92.95(1)	S1–Cu–S2	89.90(2)	S1–Cu1–S2	92.38(6)
N2–Cu–S2	85.09(5)	N2–Cu–S2	86.42(0)				
N3–Cu–S1	132.78(2)	N3–Cu–S1	110.96(1)				
N3–Cu–S2	133.65(8)	N3–Cu–S2	154.86(2)				
S1–Cu–S2	93.47(9)	S1–Cu–S2	93.97(8)				

Table S3. Diffusion coefficients for Cu(I) and Cu(II) Species

Copper complexes	D ($\times 10^{-6}$ cm^2 s^{-1})
$[Cu(N_2S_2)]_2(PF_6)_2$	8.30
$[Cu(N_2S_2)]_n(BF_4)_n$	6.17
$[Cu(N_2S_2)(CH_3CN)](PF_6)_2$	5.14
$[Cu(N_2S_2)(CH_3CN)](BF_4)_2$	5.37

Table S4. Photovoltaic parameters of the best DSCs devices based on electrolytes E1 and E2 measured under indoor-light conditions at 1000 lux.

Electrolytes	V_{oc} (V)	J_{sc} (μA cm^{-2})	FF	*PCE* (%)
E1	0.66	143.95	0.69	21.6
E2	0.66	114.77	0.68	17.0

Table S5. EIS Parameters from 10 best DSCs based on electrolytes E1 and E2.

Electrolytes	R_{rec} (Ω)	C_{μ} (mF)	τ_e (ms)
E1	235.9 ± 3.2	0.115 ± 0.010	27.12 ± 2.7
E2	176.9 ± 4.0	0.106 ± 0.013	18.75 ± 2.8

References

1 Sheldrick. G. M, *SHELXTL97 Program for the Refinement of Crystal Structure*, University of Göttingen, Germany, **1997**.

2 *Software packages SMART and SAINT*, Siemens Energy & Automation Inc., Madison, Wisconsin, **1996**.

3 Sheldrick. G. M, SADABS Absorption Correction Program, University of Göttingen, Germany, **1996**.

4 M. Hu, J. Shen, Z. Yu, R.-Z. Liao, G. G. Gurzadyan, X. Yang, A. Hagfeldt, M. Wang and L. Sun, *ACS Appl. Mater. Interfaces*, 2018, **10**, 30409.

5 Y. Zhao, J. Shen, Z. Yu, M. Hu, C. Liu, J. Fan, H. Han, A. Hagfeldt, M. Wang and L. Sun, *J. Mater. Chem. A*, 2019, **7**, 12808.

6 H. Rui, J. Shen, Z. Yu, L. Li, H. Han and L. Sun, *Angew. Chem. Int. Ed.*, 2021, **60**, 16156.

7 H. Tian, Z. Yu, A. Hagfeldt, L. Kloo and L. Sun, *J. Am. Chem. Soc.*, 2011, **133**, 9413.